Chapter 7 – Transport

There are three major transport issues that impact the NCSX design. First, is the energy confinement (with the available heating power) sufficient to reach the MHD stability limit? Second, is the configuration sufficiently quasi-axisymmetric to reduce the neoclassical ripple transport to low levels, thereby allowing tokamak-like transport? Third, is the expected pressure profile stable for $<\beta> \sim 4\%$?

The energy confinement needed to achieve the $<\beta>=4\%$ design goal is assessed chiefly through the required enhancement factor, H, over a standard stellarator scaling, ISS-95 [1], and the latest tokamak L-mode scaling, ITER-97P [2]. Comparison with a tokamak scaling is also warranted because the high degree of quasi-axisymmetry effectively eliminates ripple transport, thereby reducing the neoclassical energy transport to essentially axisymmetric levels. As a result, NCSX may have tokamak-like transport and the ITER-97P L-mode scaling may be an appropriate predictor of the 'low'-mode confinement in NCSX. The experimental basis for these scalings is briefly reviewed in Section 7.1.1. The experimental validation of neoclassical transport in stellarators is reviewed in Section 7.1.2 because neoclassical transport plays a significant role in the local transport assessment described in Section 7.3. Enhanced confinement (above the ISS-95 scaling) is seen in many stellarators, and is discussed in Section 7.1.3.

In Section 7.2 we present an overview of the confinement required for NCSX; this is assessed using a 0-D model with fixed profile shapes based on the profile predictions of a power balance code (see Section 7.3). The global confinement scaling assessment is supplemented with temperature profile predictions based on solutions of the power balance equations using a combination of neoclassical and anomalous transport; these calculations are described in Section 7.3. The predicted pressure profile shapes are within the range used in MHD stability studies. The power balance analysis finds that the NCSX design point is 'neoclassically accessible' and that the energy transport due to field ripple is much smaller than the axisymmetric neoclassical transport.

7.1 Experimental Basis for Projected Confinement

There are several ways to estimate the confinement of a new configuration. Empirical global scaling relations summarize a wide body of experience, but their extrapolability to a new type of device is unclear. Neoclassical transport theory is expected to set a lower bound on transport, and many stellarator experimental plasmas are at, or near, this lower bound. There are no widely validated models for anomalous transport in stellarators, so the anomalous transport models we use in Section 7.3 are described there.

7.1.1 Global Energy Confinement

The ISS-95 [1] global confinement scaling represents typical confinement in unoptimized stellarators with H-mode discharges excluded. This scaling is based on the 'diamagnetic' stored energy (~total stored energy, including fast ions) and the estimated actual heating power (not the injected power), so we use the corresponding quantities in assessing $H_{ISS\text{-}95}$ for NCSX. The fast ion contribution to the stored energy can reach ~25-30% of the total in low collisionality

<β>=4% NCSX plasmas, which is similar to the fast ion stored energy fraction in neutral beam heated, low density stellarator (and tokamak) plasmas.

Plasmas heated by neutral beam injection and by RF waves at the electron cyclotron resonance are included in the ISS-95 database. No confinement difference has been linked to the heating method, but in the database the heating method and density are systematically correlated (higher density plasmas are heated predominantly by NBI). There is a further correlation between density and heating power: they rise together; it was possible to determine separate dependences on density and heating power for only some of the devices.

Many NCSX parameters lie within the range of the stellarator experiments that make up the ISS-95 database. The exceptions are the minor radius, NCSX is nearly 20% larger than ATF, the aspect ratio, which is lower than that of CHS, and the heating power, at 6 MW, is twice the maximum in the ISS-95 database.

Subsequent to the development of the ISS-95 scaling, LHD [3, 4] has provided confinement data for a much larger stellarator with a minor radius up to twice the size of NCSX (and 10 times its volume), and with slightly more heating power than planned for NCSX. Energy confinement in LHD has ranged beyond twice the ISS-95 expectation [5, 6] even at high <β> [4, 7], and has no apparent dependence on heating method [8]. The enhanced confinement is attributed to an edge temperature pedestal [9, 10, 11], which is not generally observed in other stellarators but is *not* attributed to an H-mode in LHD. The pedestal may be associated with a chain of magnetic islands at or near the plasma edge [9], while avoidance of island chains at low order rational ι values is associated with H-modes in W7-AS [12, 13].

The ITER-97P L-mode energy confinement scaling [2] is based on data from many tokamaks, and fits each tokamak individually as well or better than the earlier ITER-89P scaling [14]. Most parameter ranges (e.g., size, aspect ratio, B_o, density, P_{heat}, <β>) encompass the NCSX design point. The exceptions are that the magnetic shear differs dramatically from that in NCSX, q(a) is lower in NCSX, and in the tokamaks all of the rotational transform is created by internal currents. In evaluating $H_{ITER\text{-}97P}$ for NCSX we use an effective plasma current, I_p^{eff}, which produces the same q(a) in an equivalent axisymmetric configuration. For the CDR configuration I_p^{eff} =0.48 MA (R_o/1.4 m)(B_o/1.2 T).

The NCSX goal of <β>=4% with P_{heat}~4.6 MW (R_o=1.4 m, and B_o=1.2 T with the CDR configuration) can be achieved with $H_{ISS\text{-}95}$=1.8 and $H_{ITER\text{-}97P}$=0.7 in a collisional, high-density plasma. (see Section 7.2). With an additional constraint that the minimum ν_i^*=0.25, the required H factors are raised: $H_{ISS\text{-}95}$ to 2.9 and $H_{ITER\text{-}97P}$ to 0.9 (see Section 7.2). While the required confinement is quite unremarkable for an equivalent tokamak, it is slightly better than has been achieved to date in unoptimized stellarators. LHD has a number of nearly steady state discharges with <β>~2% and $H_{ISS\text{-}95}$ up to 2.0 ($H_{ISS\text{-}95}$ rises to 2.4 with dW/dt ~ 0.13P_{abs}). More recently, LHD has achieved <β>=3% [15]. W7-AS reports $H_{ISS\text{-}95}$ up to 2.5 [16, 17], and in other plasmas <β>=3% [18]. NCSX is similar in size to the PBX-M tokamak, which achieved <β>=6.8% at B_o=1.1 T with 5.5 MW of neutral beam heating at $H_{ITER\text{-}97P}$ =1.7 and an estimated $H_{ISS\text{-}95}$~3.9 [19].

7.1.2 Experimental Confirmation of Neoclassical Predictions in Stellarators

Neoclassical theory sets a lower bound on the transport expected in NCSX, and provides an independent method of assessing the confinement required to achieve the design goals. In a number of instances stellarator experiments are in accord with neoclassical predictions, so these predictions are of more than academic interest. The ambipolar radial electric field is reviewed first because the ion particle and energy transport depends strongly on E_r. In the $1/\nu$ regime helical energy transport scales as $T^{9/2}$, but transport is greatly reduced by the E_r which produces ambipolar flux at either the ion root (usually $E_r<0$) or the electron root ($E_r>0$).

The neoclassically predicted 'ambipolar' radial electric field (the E_r required to produce ambipolar particle flux) is generally in agreement with observations in the core of CHS [20] and W7-AS [21, 22, 23] in the 'ion root' regime. Agreement has also been obtained in plasmas with net toroidal current and significant magnetic shear in W7-AS [24]. The general agreement even in plasmas with dominantly anomalous energy transport supports the widespread belief that anomalous transport is intrinsically ambipolar.

The common agreement with the neoclassically predicted electric field is very important because the neoclassical ripple transport is strongly dependent on E_r, particularly the ion channel. It may be possible to modify the radial electric field in NCSX with unbalanced momentum input from the neutral beams. This would allow enhancement of E_r (with little effect on ripple transport) or reduction in order to confirm theoretical predictions of enhanced transport with small E_r.

In the theoretically predicted 'electron root' regime [25] the magnitude of E_r is larger than in the 'ion root' (and E_r changes sign), so the transport is correspondingly lower than with the ion root. The electron root would be especially valuable in reactors, since the ripple transport has strong temperature dependence. W7-AS experiments have confirmed that transport is reduced by either sign of E_r [23]. The electron root is frequently predicted, but not usually observed in low-density ECRH plasmas in W7-AS [23] and CHS [26].

Realization of the electron root regime has been experimentally elusive, but it may have been achieved in CHS [27], W7-AS [24, 28] and LHD [29]. The example from LHD is of special interest because there is no non-thermal electron flux involved. In all cases the reduction in transport is less than expected from naive application of neoclassical theory; in most cases this may be due to a non-diffusive flux of ripple trapped suprathermal electrons (driven by the ECRH absorption) that is outside the standard theoretical treatments and transports substantial energy [30]. The neoclassically driven E_r may also reduce anomalous transport as it does in tokamaks, but this has only scanty support in stellarators [31].

In addition to confirmation of the predicted radial electric field, neoclassically predicted ion and electron energy transport is also frequently observed in the core of W7-AS plasmas [22, 23, 24, 32], and the core of ECRF heated CHS plasmas [26]. The transport due to ripple usually exceeds the axisymmetric component in existing stellarators [33, 26, 34]. Transport is greater than neoclassical predictions, however, in the edge of W7-AS and ECRF heated CHS plasmas. Even the core of neutral beam heated CHS plasmas is usually anomalous, but ion confinement in

the core of CHS hot-ion mode plasmas is close to neoclassical [35]. ATF reported anomalous electron energy transport even in the plasma core [36, 37], while observing the neoclassically predicted bootstrap current [38]. The anomalous transport in ATF was attributed to dissipative trapped electron mode turbulence, but a transport model based on a combination DTE and ion temperature gradient modes does not explain the CHS data [26]. No model for anomalous transport is supported by a wide set of data from stellarators.

W7-AS has achieved up to H_{ISS-95} ~2.5 [17], but these plasmas are consistent with neoclassical predictions for r/a<0.7, and the 'ambipolar E_r' is consistent with the measurements at all radii [23]. The unusually 'narrow' density profile (associated with the low-recycling conditions needed for this high confinement regime) is a key to the enhanced confinement, but not a departure from neoclassical behavior because the steeper density gradient leads to higher electric fields. The more recently discovered regime of enhanced confinement in W7-AS at very high density does not have narrow density profiles [18], and the temperatures are too low to produce significant ripple transport so anomalous transport is believed to be dominant here.

Energy transport in dimensionless scaling experiments with matched CHS and LHD plasmas (with significant anomalous contributions in both devices) found that core transport follows gyro-Bohm scaling and the outer regions had scaling between Bohm and gyro-Bohm [11, 34]. In several cases the anomalous contribution to the ion energy transport in LHD is close to or smaller than the expected neoclassical contribution [11, 34], but it is always non-negligible.

In both CHS [20] and LHD [34] 'inward shifted' configurations with slightly smaller R_o have somewhat improved energy confinement relative to the standard R_o. The improvement is attributed to smaller neoclassical orbit drifts in these inward shifted configurations, but anomalous transport is significant in the core for all R_o in both devices, and becomes small relative to neoclassical only for outward shifted LHD configurations with strongly de-optimized drift orbits.

Generally speaking neoclassical theory is reliable for predicting the 'ambipolar' radial electric field in stellarators (false predictions of the 'electron root' are a notable exception), and the resulting reduction in neoclassical ripple transport (from its level with E_r=0) has been widely validated. Neoclassical energy transport is often dominant in the core of W7-AS, but anomalous energy transport is usually significant or even dominant in the outer plasma and in the core of CHS and LHD. Unfortunately, there is no physical understanding of anomalous transport in stellarators that can indicate the conditions where it will be important.

7.1.3 Enhanced Confinement Regimes

A number of enhanced confinement regimes have been reported in stellarators; some of these appear to be similar to tokamak regimes, and the H-mode is among them [39]. In stellarator H-modes the energy confinement is enhanced modestly (no more than 30%) in W7-AS [12, 13] and CHS [40, 41, 42, 43]. Access is typically restricted to narrow ranges in ι that minimize damping of poloidal rotation at the plasma boundary by avoiding island chains [44, 45] (in W7-AS toroidal rotation is strongly damped by toroidal mirrors, but poloidal rotation is possible).

CHS reports two enhanced confinement regimes associated with a change in the radial electric field. One is a 'high ion temperature mode' [46] said to be similar to TFTR supershots and hot ion modes in JET and JT-60U; the similarity includes a sustained peaked density profile, which is rare in stellarators. The other enhanced confinement regime is a dynamic E_r bifurcation regime [47, 48, 49] with rapid variations in the magnitude of the radial electric field driven by central ECH; these appear to confirm theoretical predictions of E_r bifurcation [50].

As described above, W7-AS reports two distinct regimes of enhanced confinement. One is characterized as a low-recycling regime with 'narrow' density profiles and H_{ISS-95} up to 2.5 [16, 17]. The other is a very high-density regime with broad density profiles and H_{ISS-95} up to 2 [18].

LHD confinement is generally enhanced, with H_{ISS-95} up to 2, when operated in an inward shifted configuration [5, 6]. Perhaps this is a special confinement regime associated with the unusually high peripheral temperatures in LHD, or perhaps it is an indication that the ISS-95 scaling should be adjusted to better fit this data set.

7.2 Global NCSX Model: confinement dependence on β and density

A 0-D model is used to illustrate the relationship between several important plasma parameters in Figure 7-1. Contours of the minimum ion collisionality and confinement H factors required for a given <β> and density are shown for two neutral beam power levels. To increase reactor-relevance is desirable to test transport, stability, and bootstrap current at moderately low collisionality, but raising the density – and collisionality - reduces the H_{ISS-95} needed to reach a given <β>.

The '0-D model' which is based on the M45 configuration, with R_o=1.4 m, B_o=1.2 T, and with fixed profile shapes for density and temperature (those in Figure 7-5; note that the minimum ion collisionality is located at r~0.7a). The maximum density in the figure is at the Sudo limit [51]. The 0-D model is comprised of the following equations (powers are in MW, stored energy in MJ, B_o in Tesla, a and R_o in meters, <β> is not in %, $\bar{n}_e$ is in10^{19} /m^3):

Sudo density limit = $\{P_{heat}B_o/(R_o a^2)\}^{0.5}$ 2.5 x10^{19} /m^3
Based on Figure 7-5, the minimum ν_ι^* =0.027{ $\bar{n}_e^{\,3}R_o/(100<\beta>)^2B_o^{\,4}$ }

The stored energy (in MJ) is W_{tot}=1.5<β>$(10B_o^2/2\pi)V_p$, where $V_p=2R_o(\pi a)^2$
The energy confinement time is $\tau_E=W_{tot}/P_{heat}$, and the H factors are
$H_{ISS-95}= \tau_E /a^{2.21}R_o^{\,0.65}P_{heat}^{\,-0.59}\ \bar{n}_e^{\,0.51}B_o^{\,0.83}$ɬ$(2a/3)^{\,0.43}$ 0.079 sec
The effective plasma current needed for the ITER-97P confinement scaling is
Ip= $(B_o/1.2\text{ T})(R_o/1.4\text{ m})$ 0.48 MA, and for hydrogen plasmas (M_{eff}=1)
$H_{ITER-97P}= (W_{tot}/P_{inj})\ /(a/\sqrt{\kappa})^{0.31}R_o^{\,1.38}\kappa^{0.67}P_{inj}^{\,0.57}\bar{n}_e^{\,0.24}B_o^{\,0.2}I_p^{\,0.74}$0.037 sec, where "a/√κ" represents the tokamak definition of minor radius; the symbol "a" follows the stellarator definition, which is derived from the square root of the cross sectional area, so "a/√κ" is approximately the midplane minor radius.

Orbit losses reduce the heating power to $P_{heat}=P_{inj}$(1-0.24/sqrt{$(R_o/1.4\text{ m})(B_o/1.2\text{ T})$})

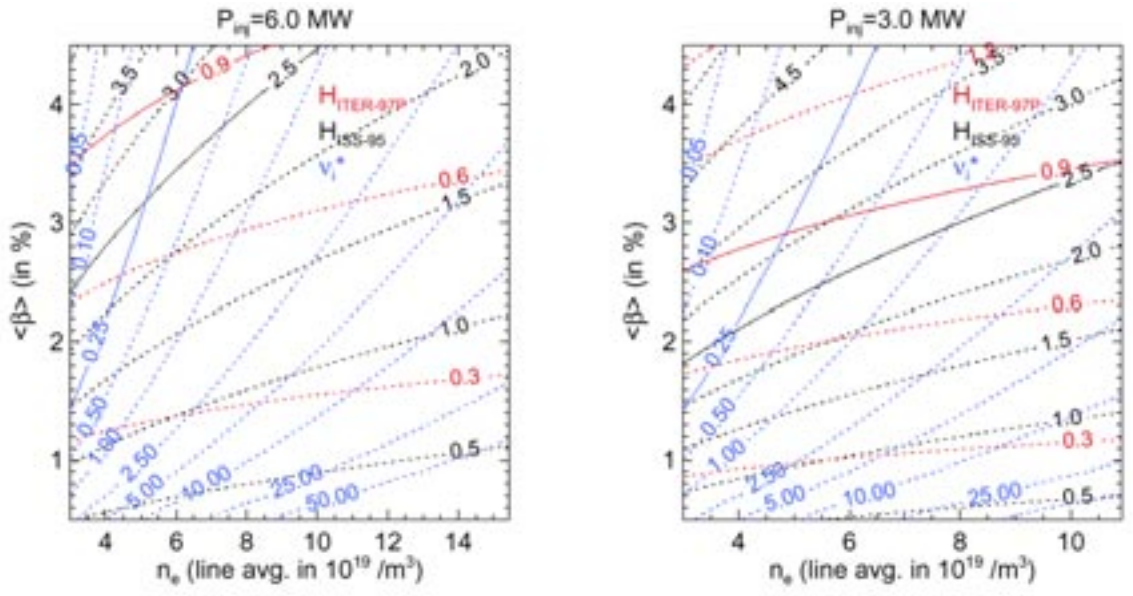

Figure 7-1. Contours of $H_{ITER\text{-}97P}$, $H_{ISS\text{-}95}$ and ν_ι* for two heating power levels.

The approximation for neutral beam orbit losses used above is based on the B_o and R_o scans in Chapter 6, which used the plasma parameters of Figure 7-5. Higher density, colder plasmas (as in Figure 7-6) will have less orbit loss because there is less time for stochastic diffusion and because the slowing down rate is increased more than the pitch angle scattering rate; no 'credit' for this is taken in the expression for the orbit loss that is used here.

As <β> is raised at a fixed density in Figure 7-1 the stored energy and H factors rise linearly with <β>, and the collisionality drops as $1/<\beta>^2$. The density dependence of the ISS-95 scaling lowers $H_{ISS\text{-}95}$ as the density rises, but the collisionality increases as $\bar{n}_e^{\,3}$ at fixed <β>. The maximum value on the density axis corresponds to the Sudo density limit.

With 6 MW of injected power the confinement required to reach a given condition is minimized. To reach <β>=4% and ν_ι*=0.25 requires $H_{ISS\text{-}95}$=2.9 and $H_{ITER\text{-}97P}$=0.9. Raising the density to the Sudo limit lowers $H_{ISS\text{-}95}$ to 1.8 at <β>=4%, but then ν_ι*>1 and the results are less relevant to subsequent devices. Finally, with confinement at the level of $H_{ISS\text{-}95}$=1, the achievable <β> is ~2.2% at the Sudo density limit. Note that $H_{ITER\text{-}97P}$ is below 1 for <β>=4% and ν_ι*=0.25, and is even lower for the other conditions described here.

With the initial capability of 3 MW injected, <β>~3.3% and ν_ι*=0.25 can be achieved with $H_{ITER\text{-}97P}$=1.0, and $H_{ISS\text{-}95}$=2.9 is compatible with <β>~2.6% and ν_ι*=0.25 (this $H_{ISS\text{-}95}$ is sufficient for <β>=4% and ν_ι*=0.25 with 6 MW of heating). And finally, with confinement at the level of $H_{ISS\text{-}95}$=1, the highest <β> is ~1.4% at the Sudo density limit.

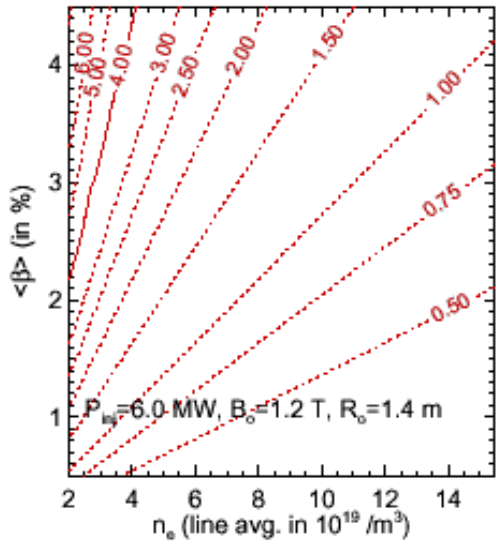

Figure 7-2 Contours of central temperature for B_o=1.2 T.

As shown in Chapter 8, the independently powered modular coils provide sufficient shaping flexibility to vary the MHD stability limit down to 1%. It is therefore possible to begin testing MHD stability predictions early with 3 MW at H_{ISS-95}~1.5; if confinement is at the level of H_{ISS-95}~1 the full beam power of 6 MW is sufficient to demonstrate stability at $\langle\beta\rangle$=2.2%. Higher levels of confinement or heating power (~6-8 MW of RF power could be added) are needed to reach the more interesting $\langle\beta\rangle$ limits of 4% or greater, but this is a plausible target since existing unoptimized stellarators reach H_{ISS-95}~2-2.5.

The central temperature in this space is indicated in Figure 7-2; the relationship between $\langle\beta\rangle$, density, and central temperature is based on the profile shapes in Figure 7-5. The contours in this figure are correct for any heating power, but the maximum on the density axis is the Sudo limit for 6 MW. Note that with high densities the temperature is generally below a keV, and impurity radiation can easily become a problem because impurities are not completely stripped of their electrons.

7.3 Transport simulations of NCSX

One of the NCSX design goals is to reduce transport by producing a highly quasi-axisymmetric configuration with the transport of an equivalent axisymmetric device. With low 'effective' ripple the neoclassical particle, energy, and momentum transport should all be reduced relative to unoptimized stellarator designs, and should be similar to tokamak transport. Anomalous transport may be reduced by the effects of flow shear and the rotational transform and magnetic shear, which are similar to those of the 'reversed shear' enhanced confinement regime in tokamaks.

The temperature prediction code described in this section also determines the self-consistent radial electric field, E_r, which would be set up by ambipolar neoclassical ripple transport. The ion energy and particle transport are strongly dependent on E_r, so the self-

consistent value must be used. The analytic estimate for E_r has been spot checked by a Monte Carlo transport calculation with GTC. With this ambipolar E_r the DKES code confirms that the transport approaches the axisymmetric neoclassical result. The benchmarks with GTC and DKES are presented in Section 7.3.2.

7.3.1 Methodology for local transport simulations

Temperature profile predictions for NCSX involve several steps:

1) estimate the E_r necessary for ambipolar particle flux,
2) estimate the ripple, axisymmetric, and anomalous transport diffusivities,
3) predict temperature profiles, and then iterate all three steps until convergence occurs.

The temperature profile predictions are solutions of the coupled power balance equations for the electron and ion temperatures. The thermal diffusivities are made up of three parts: neoclassical ripple transport, neoclassical axisymmetric transport, and an anomalous transport model with an adjustable coefficient.

The ripple transport depends on the density and temperature – and their gradients - as well as the radial electric field that, in turn, depends on the helical particle transport. Everything must be solved for 'simultaneously', so an iterative procedure is used until the temperatures and transport fluxes have converged. By construction, the algorithm for finding the ambipolar electric field searches for an ion root (the ion root occurs in almost all stellarator plasmas).

The analytic model for neoclassical helical transport used here [52, 50, and earlier references therein] is based on a 'single helicity' magnetic configuration. Mynick [53] used a Monte Carlo transport simulation to approximately verify related transport expressions for a single helicity magnetic configuration, and Beidler has also verified that similar expressions adequately describe neoclassical transport is a number of actual stellarator configurations [54, 55, 56].

The single helicity analytic model has been extended in the $1/\nu$ regime to more complex magnetic configurations [57] and benchmarked against Monte Carlo transport calculations [58]. The analytic transport model we are using applies the 'effective helical ripple' (as calculated by the NEO code [57] for the M45 configuration) to all transport regimes. A more accurate analytic model will be used in future (that described in Ref. 56), but helical transport is quite unimportant in NCSX and the impact on the predictions is expected to be small. The effective helical ripple for the M45 configuration is shown in Figure 7-3. For comparison, the effective helical ripple of W7-X is close to 0.01 at all radii, and that of ATF ranged from 0.3 near the edge to ~0.1 deep in the core.

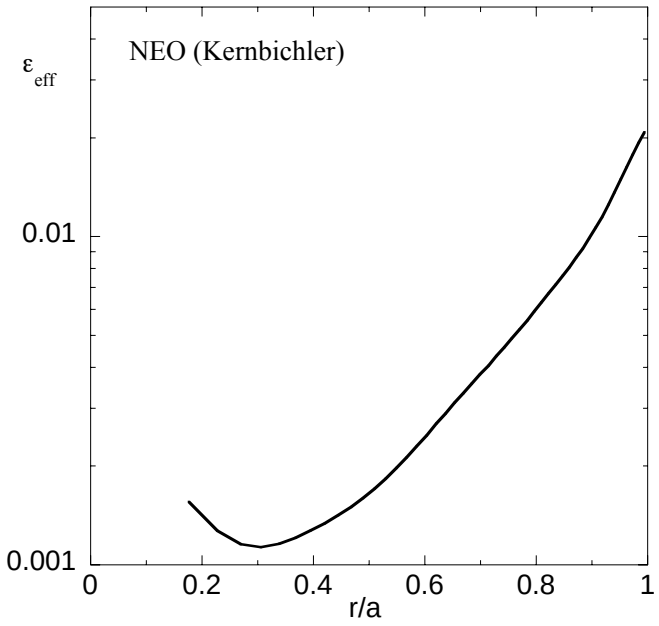

Figure 7-3. The effective helical ripple for the M45 configuration vs the square root of the normalized toroidal flux

The neoclassical axisymmetric transport is given by the Chang-Hinton [59] formulation for a circular plasma cross section; the implementation was adopted from SNAP [60]. A calculation by NCLASS (based on profiles close to those in Figure 7-5) shows that the Chang-Hinton formulation of axisymmetric transport should be reduced by 35% for these conditions, so this correction factor was used in the calculation of the Figure 7-5 profiles. Other collisionality regimes, such as that in Figure 7-6, may require a different correction; no correction was used for Figure 7-6. In future, the neoclassical transport routines in NCLASS will be incorporated into the power balance code to obtain a proper calculation of axisymmetric transport, which is expected to be more important that the helical transport in almost all conditions of interest for NCSX.

The anomalous diffusivity is adjusted in the predictions in order to match a target thermal $<\beta>$ or H factor. The power conducted by the anomalous term can then be compared to the neoclassical conduction power as a measure of confinement 'robustness'. Errors in the neoclassical models will therefore cause errors in the degree of robustness and minor changes in profile shapes, but not the overall temperature magnitudes because these are determined by the target thermal $<\beta>$ or H factor. The simplest anomalous transport model is spatially uniform. Stellarators often have experimentally determined thermal diffusivities that are approximately radially constant (unlike many tokamaks). A local Lackner-Gottardi expression for anomalous transport can also be used. This anomalous transport model is based on one originally developed for ASDEX [61], with additional B_o and R_o scaling inspired by the Lackner-Gottardi global scaling [62], and its use in a simulation of one W7-AS discharge has been reported [63]:

$$\chi^{LG} = 1.5\ m^2/s\ (1.6\ m/R_o)(2\ T/B_o)^2\ T_{e,keV}^{1.5}/(1.1-(r/a)^2)^4\ . \qquad (7\text{-}1)$$

The multiplier used here is the same for the electron and ion diffusivities, and only the temperatures near the edge are sensitive to which species has anomalous transport. This anomalous model increases strongly in the outer region of the plasma; as a result it is the dominant term only near the edge and its contribution is insignificant in the plasma core with the multipliers used here (see Figure 7-5).

The power balance solver described above has been used in TRANSP to developing the discharge evolution described in Chapter 9. The anomalous diffusivity was dynamically adjusted to meet a target τ_E that was the smaller of the L-mode scaling and neo-Alcator scaling [64]; the latter applies in the low-power ohmically heated phase of the discharge when the L-mode scaling predicts large τ_E.

The 'triangular' heating profile used here is similar to those calculated by TRANSP (see Figure 10-28) for neutral beam injection into an axisymmetric torus with the oblate portion of the NCSX cross section. The orbit loss calculations in Chapter 6 are carried out for the full 3-D geometry, and show relatively weak dependence on the injector's toroidal location, so the heating calculation in axisymmetric geometry may be a good approximation to a 3-D heating calculation. The heating power is split between ions and electrons according to the Stix thermalization model [65].

The power balance equations are solved with an assumed density profile shape, and assumed outer boundary temperatures. The resulting temperature profiles are not sensitive to variations in these assumptions, largely because the anomalous transport multiplier is adjusted until the predictions match a target (typically $<\beta>=4\%$). Where the anomalous multiplier goes to zero defines the boundary of the 'neoclassically accessible' region. For a B_o scan at $<\beta>=4\%$ the neoclassical boundary is above the maximum magnetic field of the current R_o=1.4 m design.

7.3.1 Benchmarks of analytic and numerical neoclassical transport

Reality is more complex than the analytic neoclassical transport model used in the power balance solutions in several important ways. Real stellarators have multiple helicity components, and in some stellarators there is no single dominant component. In complex configurations there will generally be multiple trapped particle populations, and each can have transport resonances where the electric and magnetic contributions to the poloidal drift cancel (see Figure 1 of Ref. 32).

The most complete numerical simulations of neoclassical transport in multi-helicity magnetic geometry use Monte Carlo methods [66, 53, 67, 68] or are based on a drift kinetic equation solver, DKES [69, 70]. All of these codes have shown that analytic theory is reliable in simple magnetic geometry. Both kinds of codes have also been used to show that the various analytic transport regimes can frequently be identified in the mono-energetic diffusivities obtained for complex geometries, although the coefficients must be fitted to the numerical results [68, 71]. The coefficient for the $1/\nu$ regime can be accurately evaluated [58] for multi-helicity magnetic configurations by the NEO code [57], which provides an 'effective helical ripple' valid in the $1/\nu$ regime. Not all energies and species are in the $1/\nu$ regime, however, so we have carried out further benchmarks for NCSX.

Maassberg [30] used the DKES[69, 70] code to calculate the mono-energetic transport coefficients at r=0.5a and 0.7a for the M45 configuration (see Figure 7-4). In the low collisionality regime, the normalized particle transport coefficient, Γ_{11}^*, approaches the equivalent axisymmetric result as the electric field is increased; and the expected magnitude of E_r/Bv is greater than the 3 10^{-3} level. With the electric fields required for ambipolar flux (as determined above) the transport will be very close to the axisymmetric result. The bootstrap coefficient, Γ_{31}, is not far from the axisymmetric result (although the latter is not the limit for large E_r) and shows much less dependence on E_r that is usual for stellarators, but is typical of tokamaks.

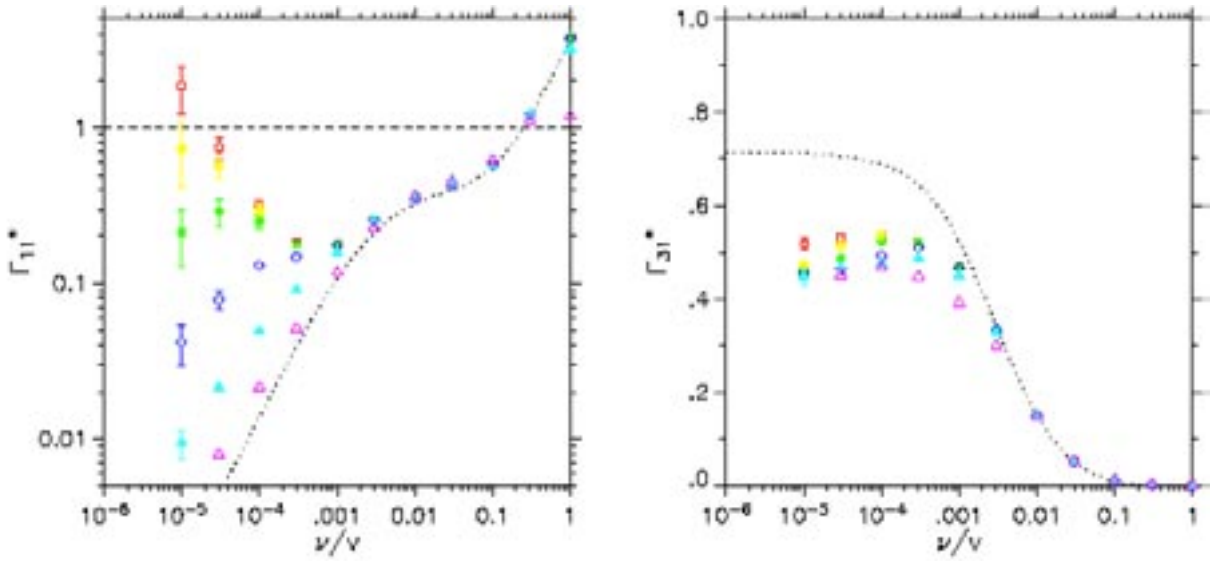

Figure 7-4. DKES results for NCSX (M45) at r=a/2: (a) mono-energetic particle transport coefficient normalized to the plateau value of an equivalent elongated axisymmetric configuration, and (b) the normalized bootstrap current coefficient. The abscissa is the inverse of the mean free path. Radial electric field values: $E_r/(Bv)$= 0 red squares, 3x10^{-4} yellow filled diamonds, 1x10^{-3} green circles, 3x10^{-3} dark blue diamonds, 1x10^{-2} blue filled triangles, 3x10^{-2} pink open triangles. Dotted curves are the axisymmetric result.

The DKES benchmark thereby confirms that neoclassical ripple transport is expected to be insignificant in the planned NCSX conditions. This conclusion could conceivably become invalid if strong central electron heating were used in NCSX; the resulting high central electron temperatures would dramatically increase the ripple fluxes, but even in this case the ripple fluxes would be small in the cooler plasma outside the center.

7.3.2 Temperature Profiles for NCSX Scenarios

Figure 7-5 shows plasma profiles for the 'standard' high <β> condition (P_{inj}=6 MW, B_o=1.2 T, R_o=1.4 m), where the density has been chosen so that the minimum ν_ι^*=0.25. Truly 'reactor relevant' collisionality values would require much higher H-factors (or B_o, or P_{inj}), but this plasma is expected to be in the relevant collisionality regime from the point of view of energy transport and bootstrap current generation. The pressure profile is within the range used

for MHD stability studies in Chapter 8. With the highly quasi-axisymmetric magnetic geometry the ripple energy transport is negligible compared to the axisymmetric neoclassical transport, which has been normalized to an NCLASS calculation for these conditions. Thus, the transport is that of an equivalent tokamak. The radially constant anomalous transport diffusivity has been used to determine how much anomalous transport can be tolerated in the plasma core. The anomalous transport exceeds the neoclassical transport in the outer two thirds of the plasma. The radial electric field is in the 'ion root' regime everywhere. (The collisionality scaling used in Section 7.2 is based on this figure.)

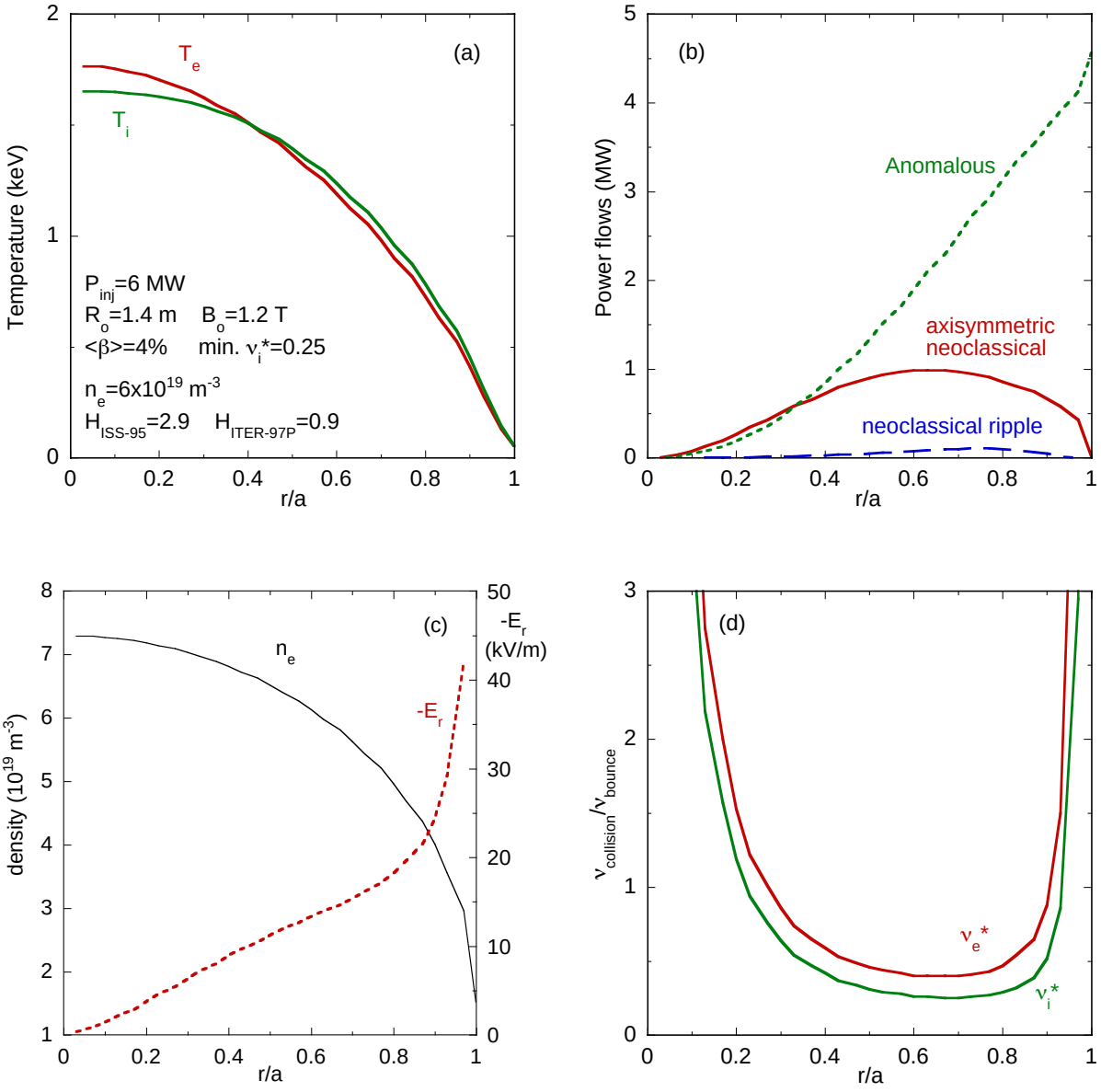

Figure 7-5. Profiles for standard high beta plasma.

When matching a target for <β>, H_{ISS-95}, or $H_{ITER-97P}$, the fast-ion stored energy is not calculated by the power balance code. In plasmas with minimum ν_ι*=0.25 the fast ion stored energy is ~25% of the total, so the target for the thermal <β> is 3%. A separate calculation using the profiles of Figure 7-5 confirmed that the total <β>, including fast ions, is 4.1%.

While the neutral beams heat ions preferentially, the neoclassical losses are also larger in the ion channel so $T_e > T_i$ in the plasma center. At larger radii $T_e < T_i$ because we have assumed the electron and ion anomalous thermal diffusivities are equal. If all the anomalous transport is assigned to one channel then it becomes the colder species where anomalous transport is dominant.

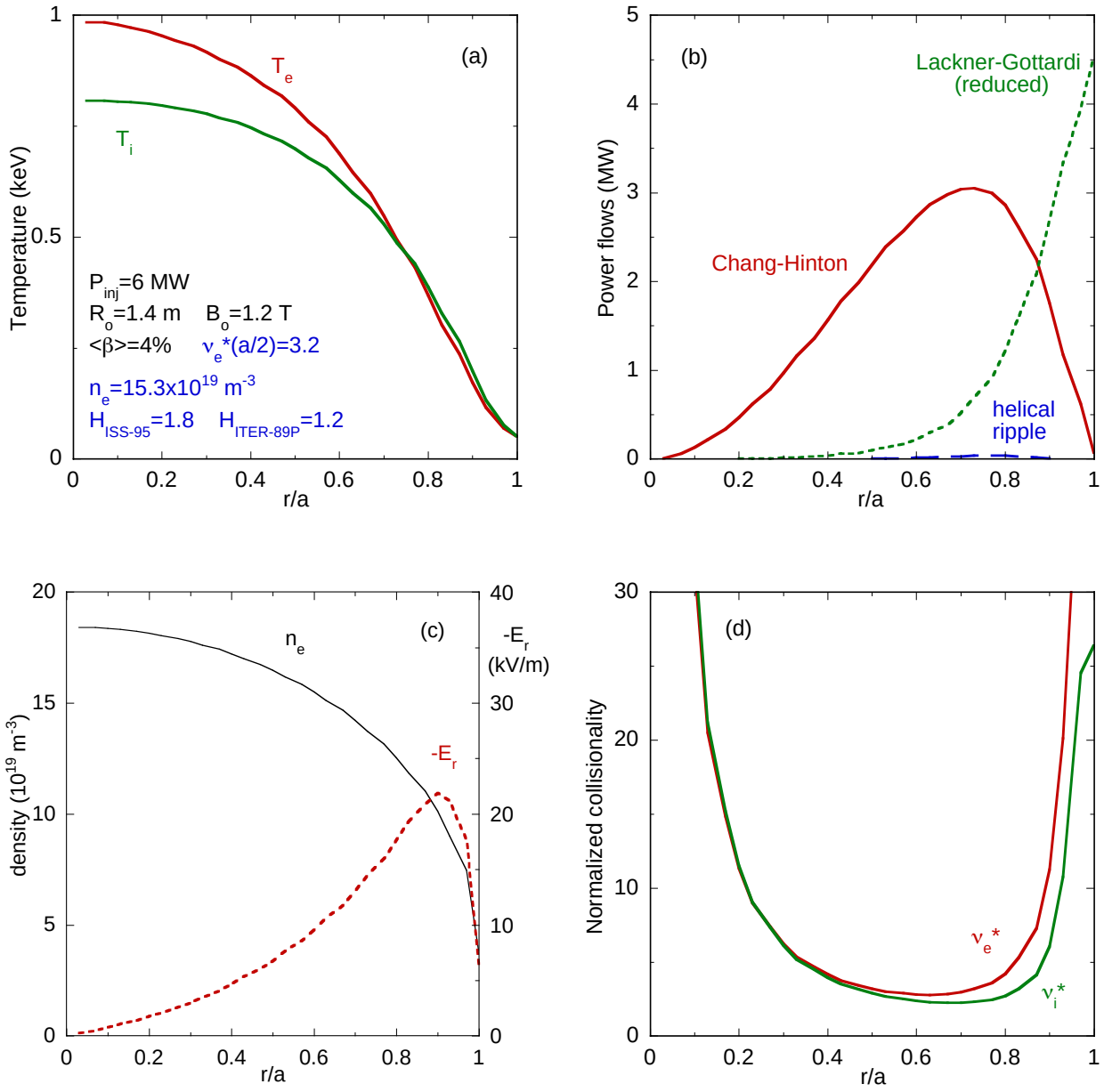

Figure 7-6. Profiles for high density, high beta plasma

The density dependence of the ISS-95 scaling favors operation at high density. Raising the density to the Sudo limit reduces the H_{ISS-95} needed to reach $<\beta>=4\%$ from 2.9 to 1.8 (see Figure 7-6). Ripple transport is even more unimportant at these lower temperatures because it has stronger temperature dependence than axisymmetric transport. The Lackner-Gottardi transport model was used, so anomalous transport is important only in the outer part of the plasma. The thermal beta is fully 4%; the fast ion contribution will be much lower in this colder denser plasma. Note that the collisionality is now high, however. These results of the power balance code are similar to those from the 0-D model in Section 7.2.

If the anomalous transport is sufficiently high to reduce H_{ISS-95} to 1, then 6 MW injected into a plasma at the Sudo density limit produces $<\beta>=2.2\%$ - enough for tests of the lower $<\beta>$ limits with unoptimized shapes (see Chapter 8). At these colder temperatures the ripple transport is reduced further and the Lackner-Gottardi anomalous model is dominant in the outer 30% of the minor radius.

The initial complement of neutral beam injectors will generate 3 MW and would be expected to produce lower $<\beta>$ for a given H factor. Again choosing the density so that minimum $\nu_\iota^*=0.25$, we find that $H_{ISS-95}=2.9$ or $H_{ITER-97P}=0.9$ implies $<\beta>=2.5$-2.8%, respectively, at $B_o=1.2$ T. This is again consistent with the 0-D results above, and would exceed the lower $<\beta>$ limits which are predicted for less optimized shapes.

7.6 Summary

We find that the high degree of quasi-axisymmetry of the M45 configuration reduces the neoclassical ripple transport to a small fraction of the neoclassical axisymmetric transport (in fact, this is true for all tested NCSX configurations). It is assumed here that the actual radial electric field (including any driven by unbalanced neutral injection) reduces the ripple transport at least as much as the 'ambipolar' electric field would. This means that NCSX is tokamak-like in the sense of being dominated by axisymmetric transport. Since the magnetic shear is similar to the 'reversed shear' enhanced confinement regime in tokamaks, it may have low levels of anomalous transport as well.

Relative to the ISS-95 global energy confinement scaling, the confinement required to reach the high $<\beta>$ goal of 4% - and low collisionality, simultaneously - is slightly higher than that already achieved in unoptimized stellarators. This level of confinement is ~10% lower than predicted by the ITER-97P tokamak L-mode scaling. By operating near the stellarator density limit, the required enhancement over the ISS-95 scaling is reduced by 35%.

A combination of neoclassical and anomalous transport models predicts pressure profile shapes that are within the range of those used to study the MHD stability of NCSX. They also show that $<\beta>=4\%$ plasmas are 'neoclassically accessible', and can tolerate large levels of anomalous transport in the outer region of the plasma. Core temperatures of up to ~2 keV are expected in plasmas with moderate collisionality.

The high degree of quasi-axisymmetry in NCSX is expected to greatly reduce the rotation damping that is usually observed in stellarators. This may result in 'tokamak' levels of flow and the potential for highly sheared flows that could reduce transport (calculations of toroidal flow

damping rates are in progress). With balanced co and counter beams it will be possible to vary the external momentum input and, hence, the flow shear to study its effects on transport.

The initial complement of 3 MW of neutral beam injection power will be sufficient to produce $<\beta>$=2.6-2.9% at B_o=1.2 T (assuming H_{ISS-95}=2.9 or $H_{ITER-97P}$=0.9) at moderate collisionality. This would be sufficient to test the lower $<\beta>$ limits which are predicted for less optimized shapes (see Chapter 8).

Standard techniques for confinement enhancement in stellarators and tokamaks are planned. These include wall conditioning, control of wall recycling, unbalanced neutral beam injection, pellet injection, limiting regions of high flux expansion, and edge biasing.

References

[1] Stroth, U., et al., Nuclear Fusion **36** (1996) 1063.
[2] Kaye, S., et al., Nuclear Fusion **37** (1997) 1303.
[3] Iiyoshi, A., et al., Nuclear Fusion **39** (1999) 1245.
[4] Fujiwara, M., et al., 18th IAEA Fusion Energy Conference, Sorrento, 2000, OV1/4.
[5] Motojima, O., et al., Phys. Plasmas, **6** (1999) 1843.
[6] Yamada, H., 2001, private communication.
[7] Sakakibara, S., et al., submitted to Nuclear Fusion, 2000.
[8] Watari, T., et al., 18th IAEA Fusion Energy Conference, Sorrento, 2000, EX8/4.
[9] Ohyabu, N., et al., Phys. Rev. Letters, **84** (2000) 103.
[10] Narihara, K., et al., 18th IAEA Fusion Energy Conference, Sorrento, 2000, EXP5/28.
[11] Yamada, H., et al., Phys. Rev. Letters, **84** (2000) 1216.
[12] Erckmann, V., et al., Phys. Rev. Letters, **70** (1993) 2086.
[13] Hirsch, M., et al., Plasma Phys. Control. Fusion **40** (1998) 631.
[14] Yushmanov, P., et al., Nuclear Fusion **30** (1990) 1999.
[15] Motojima, O., et al., 13th Intl. Stellarator Workshop, Canberra, 2002, paper OV10.
[16] Kick, M., et al., 16th IAEA Fusion Energy Conference, Montreal, **2** (1996) 27.
[17] Stroth, U., et al., Plasma Phys. Control. Fusion **40** (1998) 1551.
[18] Weller, A., et al., 13th Intl. Stellarator Workshop, Canberra, 2002, paper OIV2.
[19] Sauthoff, N., et al., 13th IAEA Fusion Energy Conference, Washington, **1 (**1990) 709.
[20] Okamura, S., et al., Nuclear Fusion **39** (1999) 1337.
[21] Maassberg, H., et al., Plasma Phys. Control. Fusion **35** (1993) B319.
[22] Baldzuhn, J., et al., Plasma Phys. Control. Fusion **40** (1998) 967.
[23] Kick, M., et al., Plasma Phys. Control. Fusion **41** (1999) A549.
[24] Erckmann, V., et al., 16th IAEA Fusion Energy Conference, Montreal, **2** (1996) 119.
[25] Mynick, H. E., Hitchon, W. N. G., Nuclear Fusion **23** (1983) 1053.
[26] Yamazaki, K., Amano, T., Nuclear Fusion **32** (1992) 633.
[27] Fujisawa, A., et al., 16th IAEA Fusion Energy Conference, Montreal, **2** (1996) 41.
[28] Maassberg, H., et al., Phys. Plasmas, **7** (2000) 295.
[29] Ida, K., et al., 18th IAEA Fusion Energy Conference, Sorrento, 2000, EX9/4.
[30] Maassberg, H., 2000, private communication.
[31] Fujisawa, A., et al., Phys. Rev. Letters, **82** (1999) 2669.

[32] Maassberg, H., et al., Phys. Fluids, **B 5** (1993) 3627.
[33] Renner, H., et al., 13th IAEA Fusion Energy Conference, Washington, **2 (**1990) 439.
[34] Yamada, H., et al., 18th IAEA Fusion Energy Conference, Sorrento, 2000, EX6/7.
[35] Ida, K., et al., submitted to Nuclear Fusion**,** 2000.
[36] Murakami, M., et al., 13th IAEA Fusion Energy Conference, Washington, **2 (**1990) 455.
[37] Murakami, M., et al., Phys. Fluids, **B 3** (1991) 2261.
[38] Murakami, M., et al., Phys. Rev. Letters, **66** (1991) 707.
[39] Wagner, F., and Stroth, U., Plasma Phys. Control. Fusion **35** (1993) 1321.
[40] Toi, K., et al., 14th IAEA Fusion Energy Conference, Wurzburg, **2** (1992) 461.
[41] Toi, K., et al., Plasma Phys. Control. Fusion **36** (1994) A117.
[42] Toi, K., et al., 15th IAEA Fusion Energy Conference, Seville, **2** (1994) 331.
[43] Toi, K., et al., Plasma Phys. Control. Fusion **38** (1996) 1289.
[44] Hirsch, M., et al., Plasma Phys. Control. Fusion **42** (2000) A231.
[45] Jaenicke, R., et al., 18th IAEA Fusion Energy Conference, Sorrento, 2000, OV4/3.
[46] Ida, K., et al., Nuclear Fusion **39** (1999) 1649.
[47] Fujisawa, A., et al., Phys. Rev. Letters, **79** (1997) 1054.
[48] Fujisawa, A., et al., Plasma Phys. Control. Fusion **42** (2000) A103.
[49] Fujisawa, A., et al., 18th IAEA Fusion Energy Conference, Sorrento, 2000, EX6/6.
[50] Hastings, D. E., Houlberg, W. A., Shaing, K.-C., Nuclear Fusion **25** (1985) 445.
[51] Sudo, S., et al., Nuclear Fusion **30** (1990) 11.
[52] Shaing, K.-C., Phys. Fluids **27** (1984) 1567.
[53] Mynick, H. E., Phys. Fluids, **25** (1981) 325.
[54] Beidler, C. D., Hitchon, W. N. G., Shohet, J. L., J. Comp. Phys. **72** (1987) 220.
[55] Beidler, C. D., Hitchon, W. N. G., Plasma Phys. Control. Fusion **36** (1994) 317.
[56] Beidler, C. D., D'haeseleer, W. D., Plasma Phys. Control. Fusion **37** (1995) 463.
[57] Nemov, V. V., et al., Phys. Plasmas, **6** (1999) 4622.
[58] Beidler, C. D., et al., 13th Intl. Stellarator Workshop, Canberra, 2002, paper OI10.
[59] Chang, C. S., Hinton, F. L., Phys. Fluids, **29** (1986) 3314.
[60] Towner, H., et al., Rev. Sci. Instrum. **63** (1992) 4753.
[61] Lackner, K., et al., Plasma Phys. Control. Fusion **31** (1989) 1629.
[62] Lackner, K., Gottardi, N. A. O., Nuclear Fusion **30** (1990) 767.
[63] Karulin, N., "Transport modeling of stellarators with ASTRA", IPP 2/328, Max-Planck Institut fur Plasmaphsyik, Garching, Germany (December 1994).
[64] Parker, R. R., et al., Nuclear Fusion **25** (1985) 1127.
[65] Stix, T. H., Plasma Physics, **14** (1972) 367.
[66] Boozer, A. H., Kuo-Petravic, G., Phys. Fluids **24** (1981) 851.
[67] Lin, Z., Tang, W. M., Lee, W. W., Phys. Plasmas, **2** (1995) 2975.
[68] Lotz, W.,Nuehrenberg, J., Phys. Fluids, **31** (1988) 2984.
[69] Hirshman, S. P., et al., Phys. Fluids, **29** (1986) 2951.
[70] van Rij, W.I., Hirshman, S. P., Phys. Fluids, **B 1** (1989) 563.
[71] Maassberg, H., et al., Plasma Phys. Control. Fusion **41** (1999) 1135.